Propagation of Joint Space Quantization Error to Operational Space Coordinates and Their Derivatives

Nick Colonnese[1] and Allison M. Okamura[2]

***Abstract*—Many robotic systems achieve position sensing through the use of optical encoders that specify the position of a joint to a certain resolution. Encoders effectively quantize joint space coordinates and introduce position measurement error in the process. This error propagates to operational space coordinates, limiting end-effector position and orientation resolution, and also to joint and operational space coordinate derivatives, manifesting as noise that can vitiate the signal. In this paper, we characterize encoder error in a robotic system. Given encoder specifications, robot kinematics, and discrete transfer functions mapping coordinates to their derivatives, we describe the propagation of quantization error on joint space coordinates to operational space coordinates, joint space coordinate derivatives, and operational space coordinate derivatives. We establish two results for quantization error. The first is a general result useful for establishing worst-case bounds. The second models each quantization as independent additive pseudo quantization noise (PQN) for which stochastic metrics on the error are determined. Experimental data gathered from a Phantom Premium robot/haptic device supports the analytical results.**

***Index Terms*—Motion Control, Encoder Error, Robotic and Haptic Device Design**

I. Introduction

A. Quantization from Optical Encoders in Robots

FOR many robotic systems, including manipulators, mobile robots, and kinesthetic haptic devices, position sensing is achieved through the use of optical encoders mounted on each joint. Encoders are the most common position sensing method in robotics and haptics because they can feature higher reliability and precision at a lower cost compared to other position sensing alternatives, and they are easy to implement. The output of an optical encoder is a digital signal, free of external noise, that corresponds to a certain range in which the position of the joint lies (Fig. 1). Because encoders specify the position of a joint to a limited resolution (the quantization interval of the encoder), they effectively quantize joint space coordinates, and in the process, introduce error. This usually small error propagates to operational space coordinates, such as Cartesian position and Euler angles. The error is also propagated, and can be amplified, to estimates of joint or operational space coordinate derivatives, e.g., Cartesian velocity or acceleration.

*This work was supported in part by National Science Foundation grant 1217635

[1]Oculus Research, Redmond, Washington 98052. nick.colonnese@oculus.com

[2]Department of Mechanical Engineering, Stanford University, Stanford, California 94305. aokamura@stanford.edu

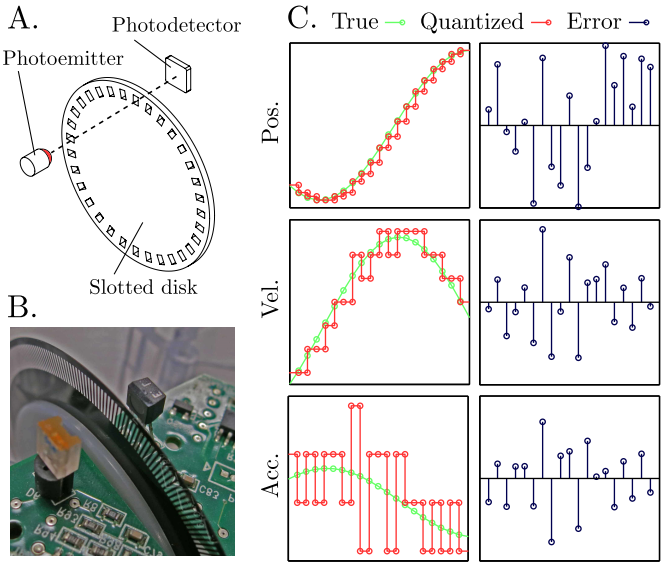

Fig. 1. A. Schematic of an optical encoder: a photoemitter and photodetector pair sit on opposite sides of a slotted disk. B. The optical encoder setup on the joint of a Falcon haptic device (Novint Technologies, Inc.). C. True, quantized, and error on position, velocity, and acceleration signals.

In a broad array of robotic applications, in which a robot must be controlled accurately and precisely, signals derived from quantized joint positions are used for control. These applications include pick and place, tracking, haptic virtual environments, teleoperation, and many others. The feedback control algorithms used for these applications commonly rely on operational space coordinates, as well as estimates of their velocities. In these scenarios, the error introduced by quantization from encoders in joint space can be a limiting factor on performance in two main ways. The first is that the encoders determine the position and orientation resolution for the robot in joint space, and contribute to the resolution (along with gearing and kinematic structure) in operational space. A baseline resolution for operational space coordinates assuming rigid kinematic linkages is determined by encoder quantization. The second limiting factor is that error introduced by quantization in joint space coordinates is amplified when derivative estimates are formed, manifesting as noise. The magnitude of the noise can be difficult to establish theoretically, and is usually found experimentally. For applications with strict requirements, e.g., haptic velocity rendering, this makes design cumbersome and requires iterations.

B. Background

This analysis draws on the results of quantization theory and the propagation of noise in linear systems. To our knowledge, applying quantization theory to determine error from optical encoders has not been considered. No worst-case, or average, quantization error results exist for a robotic system in which many sources of quantization combine to many outputs.

A coherent analysis of single-input, single-output (SISO) quantization theory is presented by Widrow and Kollár [1]. Bennett first proposed a model of additive white noise (or pseudo quantization noise, PQN) from which stochastic results are established for the error distribution [2]. Widrow popularized this approach, and described how quantization error propagates through a linear system [3]. Conditions for the validity of the PQN model were established in prior work [4], [5], [6], [7]. The worst-case model of quantization error was initially proposed by Bertram [8].

In our analysis, the propagation of quantization error through diagonal multiple-input, multiple-output (MIMO) transfer functions is accomplished using the propagation of power spectral densities [9], and transfer function norms [10]. Specifically, worst-case and stochastic error results are presented in the form of ℓ_1 and H_2 norms of transfer functions, respectively. Because they are expressed explicitly as transfer function norms, they can be used in modern optimization techniques [11].

Prior work has examined derivative error on discrete quantized coordinates from optical encoders. Kavanagh and Murphy presented variance and spectral error characteristics for a quantizer with a constant rate input subject to additive uniform noise [12]. Brown et al. investigated algorithms for velocity estimation and established relative accuracy and error of various methods based on numerical simulations and experiments [13]. Phillips and Branicky also compared velocity estimation algorithms, in which they derived upper bounds on absolute and relative errors for each of the algorithms under constant velocity and acceleration [14]. Harrison and Stoten presented a method to estimate arbitrary derivative order using truncated finite difference schemes [15].

Our analysis is applicable to all robots with quantized joint space coordinates, but is particularly relevant to kinesthetic (force-feedback) haptic devices using optical encoders for joint position sensing. Human vibration sensing is extremely acute, and in many haptic controller design scenarios the error introduced by quantization can be the limiting factor on the performance of the haptic display. Recent research in this field has established conditions for quantization-error passivity and limit cycles for a general haptic control law for a *single* quantization source [16]; our analysis in this paper expands those results to an arbitrary number of quantization elements.

C. Contributions

In this paper, we characterize encoder error in a robotic system. Given encoder specifications, robot kinematics, and discrete transfer functions mapping coordinates to their derivatives, we describe the propagation of quantization error on joint space coordinates to operational space coordinates, joint space coordinate derivatives, and operational space coordinate derivatives. We propose two models for quantization error in joint space. The first model is a general one useful for establishing worst-case bounds on the error. The second case, which models quantization as additive PQN sources, establishes stochastic metrics on the error, i.e., mean vectors and covariance matrices.

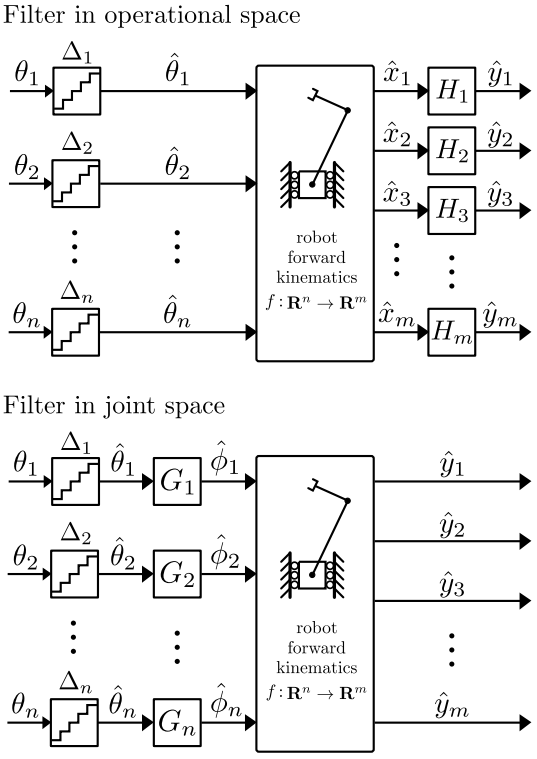

Fig. 2. Two common architectures to obtain operational space coordinate derivative estimates from joint space coordinates. Quantized joint space coordinates $\hat{\theta}$ have error that propagates to operational space coordinates $\hat{x}$, joint space coordinate derivative estimates $\hat{\phi}$, and operational space coordinate derivative estimates $\hat{y}$. Operational space coordinate derivative estimates can be formed by filtering in operational space (A), or filtering in joint space (B).

II. System Model

Table I lists the notation used. Fig. 2 shows two system diagrams representing common methods to form derivative estimates on operational space coordinates. By operational space, we refer to any coordinates derived from the joint coordinates of the robot. Common operational space coordinates include Cartesian position or Euler angles. Fig. 2 A. forms operational space coordinate derivatives by first calculating the operational space coordinates with the forward kinematics, and then inputting these coordinates into a transfer function matrix that map these coordinates to estimates of their derivatives. In contrast, Fig. 2 B. first estimates joint space coordinate derivatives using a transfer function matrix, then forms operational space coordinate derivate estimates using the forward kinematics.

In both methods, discrete-time true joint space coordinates $\theta_1, \theta_2, \ldots, \theta_n \in \mathbb{R}$ undergo spatial quantization with respective quantization intervals $\Delta_1, \Delta_2, \ldots, \Delta_n \in \mathbb{R}$, resulting in quantized joint angles $\hat{\theta}_1, \hat{\theta}_2, \ldots, \hat{\theta}_n \in \mathbb{R}$. The quantized

TABLE I
NOTATION

Symbol	Description
$\Delta \in \mathbb{R}^n$	quantization interval vector
$\theta \in \mathbb{R}^n$	true joint space vector
$\phi \in \mathbb{R}^n$	true joint space deriv. vector
$x \in \mathbb{R}^m$	true operational space vector
$y \in \mathbb{R}^m$	true operational space deriv. vector
$\hat{(.)} \in \mathbb{R}^{d(.)}$	quantized (.) vector, e.g., $\hat{\theta}, \hat{\phi}, \hat{x}, \hat{y}$
$\tilde{(.)} \in \mathbb{R}^{d(.)}$	error on (.) vector, e.g., $\tilde{\theta}, \tilde{\phi}, \tilde{x}, \tilde{y}$
$J \in \mathbb{R}^{m \times n}$	Jacobian matrix: $\dot{x} = J\dot{\theta}$
$J_i \in \mathbb{R}^m$	ith column of J
$\Sigma_{(.)} \in \mathbb{R}^{d(.) \times d(.)}$	covariance matrix of (.), e.g., $\Sigma_{\tilde{\theta}}$
G_i	joint space SISO TF at index i
H_j	op. space SISO TF at index j
G (size $n \times n$)	diagonal joint space TF matrix
H (size $m \times m$)	diagonal op. space TF matrix
$R_{(.)}(k) \in \mathbb{R}^{d(.) \times d(.)}$	autocorrelation matrix of (.)
$S_{(.)}(\omega) \in \mathbb{R}^{d(.) \times d(.)}$	power spectral density matrix of (.)

$1 \leq i \leq n$ indexes joint space coordinates, e.g. $\theta_i \in \mathbb{R}$
$1 \leq j \leq m$ indexes operational space coordinates, e.g. $x_j \in \mathbb{R}$
d(.) denotes the dimension of (.)

joint angles are mapped to operational space coordinates $\hat{x}_1, \hat{x}_2, \ldots, \hat{x}_m \in \mathbb{R}$ by the forward kinematics.

A derivative signal estimate on a joint space coordinate at index i, $\hat{\phi}_i \in \mathbb{R}$, (e.g. joint velocity or acceleration) is obtained through a single-input, single-output (SISO) discrete transfer function G_i, $\hat{\phi}_i = G_i(\hat{\theta}_i)$. Similarly, a derivative signal estimate on an operational space coordinate at index j, $\hat{y}_j \in \mathbb{R}$, is obtained through a SISO discrete transfer function H_j, $\hat{y}_j = H_j(\hat{x}_j)$. The SISO coordinate-wise filtering is equivalent to diagonal MIMO discrete transfer function matrices G (size $n \times n$) and H (size $m \times m$), which map joint and operational space coordinates, respectively, to estimates of their derivatives.

III. Error Propagation

Here we describe the propagation of quantization error on joint space coordinates to operational space coordinates, estimates of joint space coordinate derivatives, and estimates of operational space coordinate derivatives. We establish two results for quantization error. The first result is a general one useful for establishing worst-case bounds. The second models each quantization as independent additive PQN for which stochastic metrics, e.g. means and variances, on the error are determined.

A. Error on Joint Space Coordinates

The quantization operator maps an input set with an infinite number of elements to an output set with a finite number of elements. An ideal optical encoder measuring the position of a robot joint behaves as a uniform quantizer in which the output elements are all equally spaced. At a certain joint at index i, quantization operates on the true joint space coordinate, $\theta_i \in \mathbb{R}$, to return a quantized coordinate, $\hat{\theta}_i \in \mathbb{R}$. The error at this coordinate, $\tilde{\theta}_i \in \mathbb{R}$, is the difference between the quantized and true coordinate,

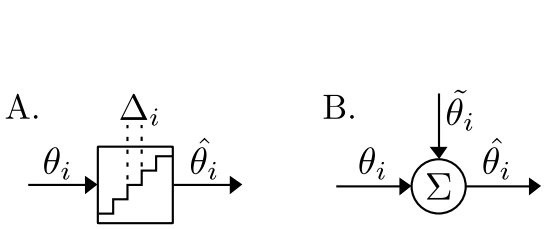

Fig. 3. Two conceptual models for quantization. A. quantization operates on true joint space coordinate at index i, θ_i, and returns $\hat{\theta}_i$ with resolution Δ_i. B. Noise $\tilde{\theta}_i \in \mathbb{R}[-\Delta_i/2, \Delta_i/2]$ is added to the true joint space coordinate to produce $\hat{\theta}_i$. For the pseduo-quantization-noise (PQN) model, the noise is white, with a uniform distribution between $-\Delta_i/2$ and $\Delta_i/2$.

$$\tilde{\theta}_i = \theta_i - \hat{\theta}_i. \tag{1}$$

Quantization introduces error on the joint space coordinate measurement, which we refer to as "noise". This noise is used as a conceptual model, and should not be confused with some additional source of error. This interpretation is shown in Fig. 3.

At joint index i, the quantized joint coordinate is always within $\Delta_i/2$ of the true joint coordinate. Thus, the error at a joint must satisfy

$$-\frac{1}{2}\Delta_i \leq \tilde{\theta}_i \leq \frac{1}{2}\Delta_i. \tag{2}$$

This can also be expressed in vector form as

$$-\frac{1}{2}\Delta \leq \tilde{\theta} \leq \frac{1}{2}\Delta. \tag{3}$$

where $\tilde{\theta} \in \mathbb{R}^n$ is a vector of the joint space coordinate errors $\tilde{\theta} = \left[\tilde{\theta}_1, \tilde{\theta}_2, \ldots, \tilde{\theta}_n\right]^T$, and $\Delta \in \mathbb{R}^n$ is a vector of the quantization intervals: $\Delta = [\Delta_1, \Delta_2, \ldots, \Delta_n]^T$. Equations (2) and (3) establish worst-case bounds for the quantization error in joint space.

If quantization on a joint space coordinate at index i is modeled stochastically as additive PQN, then $\hat{\theta}_i$ has a uniform distribution,

$$\tilde{\theta}_i \sim U(-\Delta_i/2, \Delta_i/2). \tag{4}$$

The mean of $\tilde{\theta}_i$, $\mathbf{E}\tilde{\theta}_i$, is given by

$$\mathbf{E}\tilde{\theta}_i = \int \tilde{\theta}_i p(\tilde{\theta}_i) d\tilde{\theta}_i = 0. \tag{5}$$

The variance of $\tilde{\theta}_i$, $\sigma^2_{\tilde{\theta}_i}$, is given by

$$\sigma^2_{\tilde{\theta}_i} = \mathbf{E}((\tilde{\theta}_i - \mathbf{E}\tilde{\theta}_i)(\tilde{\theta}_i - \mathbf{E}\tilde{\theta}_i)) = \Delta_i^2/12. \tag{6}$$

For the PQN model, $\tilde{\theta}$ is random vector. The mean of $\tilde{\theta}$, $\mathbf{E}\tilde{\theta}$, is given by

$$\mathbf{E}\tilde{\theta} = \mathbf{0}, \tag{7}$$

where $\mathbf{0}$ denotes the zero vector in $\mathbb{R}^n$. The covariance of $\tilde{\theta}$, $\Sigma_{\tilde{\theta}} \in \mathbb{R}^{n \times n}$, is defined by

$$\Sigma_{\tilde{\theta}} = \mathbf{E}((\tilde{\theta} - \mathbf{E}\tilde{\theta})(\tilde{\theta} - \mathbf{E}\tilde{\theta})^T). \tag{8}$$

If the error at one joint is independent of another, $\Sigma_{\tilde{\theta}}$ is given by the diagonal matrix,

$$\Sigma_{\tilde{\theta}}(i,i) = \frac{\Delta_i^2}{12} \qquad \text{for } i = 1, 2, \ldots, n. \tag{9}$$

B. Local Error on Operational Space Coordinates

Let $x \in \mathbb{R}^m$ and $\hat{x} \in \mathbb{R}^m$ be vectors representing operational space coordinates formed from true and quantized joint space coordinates, respectively, using the forward kinematics $f : \mathbb{R}^n \to \mathbb{R}^m$. The operational space error vector, $\tilde{x} \in \mathbb{R}^m$ is defined as

$$\tilde{x} = \hat{x} - x. \tag{10}$$

We use an affine approximation to the forward kinematics to describe local error propagation. Let $J \in \mathbb{R}^{m \times n}$ be the Jacobian relating joint and operational space velocities; $\dot{x} = J\dot{\theta}$. In general, the Jacobian is a function of the configuration, $J(\theta)$, but for simplicity of notation, we note it simply as J. Then

$$\begin{aligned} \tilde{x} &= \hat{x} - x, && (11)\\ &= f(\hat{\theta}) - f(\theta), && (12)\\ &\approx f(\theta) + J(\hat{\theta} - \theta) - f(\theta), && (13)\\ &= J\tilde{\theta}. && (14) \end{aligned}$$

The affine approximation of $f(\hat{\theta})$, performed at θ, is valid if the contribution of higher-order terms in $\hat{\theta} - \theta$ are negligible compared to the approximation. The $J(\hat{\theta} - \theta)$ term scales linearly with the entries of $\hat{\theta} - \theta$, while the higher-order terms scale quadratically or higher. The entries of $\hat{\theta} - \theta$ are bounded by the quantization interval Δ_i for each joint, and if the quantization intervals are sufficiently small, the approximation is valid. However, because the Jacobian is configuration dependent, the approximation is only valid locally, in the neighborhood of values close to θ.

The error at operational space coordinate indexed by j, $\tilde{x}_j \in \mathbb{R}$, must satisfy

$$-\sum_{i=1}^{n} \frac{1}{2}|J_{ji}|\Delta_i \leq \tilde{x}_j \leq \sum_{i=1}^{n} \frac{1}{2}|J_{ji}|\Delta_i, \tag{15}$$

or in vector form,

$$-\frac{1}{2}|J|\Delta \leq \tilde{x} \leq \frac{1}{2}|J|\Delta, \tag{16}$$

where $|J|$ is the element-wise absolute value of J. Equation (16) establishes a worst-case bound.

For the independent PQN model of quantization, a local description of the mean of the error vector in operational space is given by

$$\mathbf{E}\tilde{x} = \mathbf{0}, \tag{17}$$

where $\mathbf{0}$ represents the zero vector in $\mathbb{R}^m$. The local description of the covariance of the error vector in operational space is given by

$$\Sigma_{\tilde{x}} = J\Sigma_{\tilde{\theta}}J^T. \tag{18}$$

The variance of a specific operational space coordinate at index j, $\Sigma_{\tilde{x}}(j,j)$ is given by

$$\begin{aligned} \Sigma_{\tilde{x}}(j,j) &= (J\Sigma_{\tilde{\theta}}J^T)(j,j) && (19)\\ &= \left(\sum_{i=1}^{n} J_i J_i^T \frac{\Delta_i^2}{12}\right)(j,j) && (20)\\ &= \sum_{i=1}^{n} \frac{\Delta_i^2 a_i}{12}, && (21) \end{aligned}$$

where

$$a_i \in \mathbb{R} = J_i J_i^T(j,j), \tag{22}$$

and J_i is the ith column of J. Equation (21) establishes that, given a certain configuration of the robot, the variance of the error on an operational space coordinate is a linear combination of the square of the quantization intervals Δ_i^2. This representation is useful because the set of a_i for $i = 1, 2, \ldots, n$ shows the relative effect of the quantization intervals on an operational space coordinate error. If all the quantization intervals are the same, the variance of the error is proportional to the square of the quantization interval, so the standard deviation is linear in the quantization interval.

C. Error Propagation to Derivative Signals

In this subsection we establish worst-case and stochastic error results for joint and operational space derivatives. Consider SISO discrete transfer functions G_i and H_j. Here G_i maps the joint space coordinate at index i, $\hat{\theta}_i$, to $\hat{\phi}_i$, and H_j maps the operational space coordinate at index j, $\hat{x}_j$, to $\hat{y}_j$. The SISO coordinate-wise filtering is equivalent to diagonal MIMO discrete transfer function matrices, G and H, where $\hat{\phi} = G(\hat{\theta})$, and $\hat{y} = H(\hat{x})$.

The output error of the transfer functions will be the input error propagated through the transfer functions. In this analysis we are interested in transfer functions that map coordinates to estimates of their derivatives, although the approach is applicable to any transfer function matrix.

1) Worst-case derivative error results: If a transfer function is stable, given a bound on the error at the input, a bound on the error at the output can be determined using the sub-multiplicative property [17].

For bounding the error on a joint space derivative estimate at index i, $\hat{\phi}_i$,

$$\begin{aligned} \|\tilde{\phi}_i\|_\infty &= \|G_i(\tilde{\theta}_i)\|_\infty && (23)\\ &\leq \|G_i\|_{\ell_1}\|\tilde{\theta}_i\|_\infty, && (24) \end{aligned}$$

where $\|\tilde{\phi}_i\|_\infty$, $\|G(\tilde{\theta}_i)\|_\infty$, and $\|\tilde{\theta}_i\|_\infty$ are the infinity norms of the discrete time *signals*, i.e., the peak absolute value, and $\|G_i\|_{\ell_1}$ is the ℓ_1 norm of the transfer function G_i. Because the infinity norm of a signal bounds all the values of the signal, this can also be expressed as,

$$|\tilde{\phi}_i| \leq \|G_i\|_{\ell_1}|\tilde{\theta}_i|_{\max}. \tag{25}$$

Similar results exist for bounding the error on an operational space derivative estimate at index j, $\tilde{y}_j$, for both architectures shown in Fig. 2. If we use the architecture that filters in operational space,

$$|\tilde{y}_j| \leq \|H_j\|_{\ell_1}|\tilde{x}_j|_{\max}. \tag{26}$$

If we use the architecture that filters in joint space,

$$|\tilde{y}_j| \leq \sum_{i=1}^{n} |J_{ji}||\tilde{\phi}_i|_{\max}. \tag{27}$$

Equations (25), (26) and (27) establish worst-case bounds on the derivative estimates.

2) Stochastic derivative error results: Results for stochastic metrics on the derivative signal estimates, e.g. their mean and covariance, are obtained by examining the error distribution of the input, which is valid for the independent PQN model of quantization.

Because the input error to the transfer functions, $\tilde{\theta}$ and $\tilde{x}$, are zero mean, the output errors will also be zero mean,

$$\mathbf{E}\tilde{\phi} = \mathbf{0}, \tag{28}$$

$$\mathbf{E}\tilde{y} = \mathbf{0}. \tag{29}$$

To find the covariance matrices of the error on the derivative estimates, $\Sigma_{\tilde{\theta}}$ and $\Sigma_{\tilde{y}}$, the propagation of power spectral densities through transfer functions is used.

First, we establish the covariance matrix for the error on the joint space derivative estimates, $\Sigma_{\tilde{\phi}} \in \mathbb{R}^{n\times n}$. Because the error on $\tilde{\phi}$ is zero mean,

$$\Sigma_{\tilde{\phi}} = \mathbf{E}((\tilde{\phi} - \mathbf{E}\tilde{\phi})(\tilde{\phi} - \mathbf{E}\tilde{\phi})^T) \tag{30}$$

$$= \mathbf{E}(\tilde{\phi}\tilde{\phi}^T) \tag{31}$$

$$= R_{\tilde{\phi}}(0), \tag{32}$$

where $R_{\tilde{\phi}}(\tau) \in \mathbb{R}^{n\times n}$,

$$R_{\tilde{\phi}}(\tau) = \mathbf{E}(\tilde{\phi}(k)\tilde{\phi}(k-\tau)^T), \tag{33}$$

is the autocorrelation matrix of $\tilde{\phi}$. The diagonal entries of $R_{\tilde{\phi}}(\tau)$ are the autocorrelations of the n random variables, $\tilde{\phi}_1, \ldots, \tilde{\phi}_n$, and the cross terms are the cross-correlations. The relationship between the power spectral density matrix of $\tilde{\phi}$, $S_{\tilde{\phi}}(\omega) \in \mathbb{R}^{n\times n}$,

$$S_{\tilde{\phi}}(\omega) = \sum_{\tau=-\infty}^{\infty} R_{\tilde{\phi}}(\tau)e^{-j\omega\tau}, \tag{34}$$

and the covariance matrix of $\tilde{\phi}$ (with zero mean) is

$$\Sigma_{\tilde{\phi}} = \frac{1}{2\pi}\int_{-\pi}^{\pi} S_{\tilde{\phi}}(\omega)d\omega. \tag{35}$$

For $\tilde{\phi} = G\tilde{\theta}$, the input and output error power spectral densities are related by

$$S_{\tilde{\phi}}(\omega) = G(\omega)^* S_{\tilde{\theta}}(\omega)G(\omega), \tag{36}$$

where $G^*(\omega)$ denotes the complex conjugate of $G(\omega)$. In the independent PQN model, the error at a coordinate is white, so

$$S_{\tilde{\theta}} = \Sigma_{\tilde{\theta}}. \tag{37}$$

Therefore, combining Equations (35), (36) and (37),

$$\Sigma_{\tilde{\phi}} = \frac{1}{2\pi}\int_{-\pi}^{\pi} G(\omega)^*\Sigma_{\tilde{\theta}}G(\omega)d\omega. \tag{38}$$

Here $\Sigma_{\tilde{\phi}}$ will be diagonal, and can be expressed component-wise as

$$\Sigma_{\tilde{\phi}}(i,i) = \frac{1}{2\pi}\int_{-\pi}^{\pi} G_i(\omega)^* G_i(\omega)d\omega\, \Sigma_{\tilde{\theta}}(i,i) \tag{39}$$

$$= \|G_i\|_2^2\, \Sigma_{\tilde{\theta}}(i,i), \tag{40}$$

where $\|G_i\|_2^2$ is the squared H_2 norm of the transfer function G_i [17].

The covariance matrix of the error on the operational space coordinate derivative estimates $\Sigma_{\tilde{y}} \in \mathbb{R}^{m\times m}$ is found for both architectures shown in Fig. 2.

For the filter in joint space architecture, because $\tilde{y} = J\tilde{\phi}$,

$$\Sigma_{\tilde{y}} = J\Sigma_{\tilde{\phi}}J^T. \tag{41}$$

For the filter in operational space architecture, the propagation of the error power spectral densities is used to find $\Sigma_{\tilde{y}}$, similar to the approach used for finding $\Sigma_{\tilde{\phi}}$,

$$S_{\tilde{y}}(\omega) = H(\omega)^* S_{\tilde{x}}(\omega)H(\omega). \tag{42}$$

Because $\tilde{x} = J\tilde{\theta}$, the power spectral density of the input error $\tilde{x}$, $S_{\tilde{x}}(\omega)$, is given by,

$$S_{\tilde{x}}(\omega) = JS_{\tilde{\theta}}(\omega)J^T = J\Sigma_{\tilde{\theta}}J^T = \Sigma_{\tilde{x}}. \tag{43}$$

Therefore, using the relationships of Equations (42) and (43),

$$\Sigma_{\tilde{y}} = \frac{1}{2\pi}\int_{-\pi}^{\pi} S_{\tilde{y}}(\omega)d\omega \tag{44}$$

$$= \frac{1}{2\pi}\int_{-\pi}^{\pi} H(\omega)^*\Sigma_{\tilde{x}}H(\omega)d\omega. \tag{45}$$

Because of the diagonal structure of H, $\Sigma_{\tilde{y}}$ can be expressed component-wise as

$$\Sigma_{\tilde{y}}(j,j) = \int_{-\infty}^{\infty} H_j(\omega)^* H_j(\omega)d\omega\, \Sigma_{\tilde{x}}(j,j) \tag{46}$$

$$= \|H_i\|_2^2\, \Sigma_{\tilde{x}}(j,j), \tag{47}$$

for the diagonal entires, and

$$\Sigma_{\tilde{y}}(p,q) = \int_{-\pi}^{\infty} H_p(\omega)^* H_q(\omega)d\omega\, \Sigma_{\tilde{x}}(p,q) \tag{48}$$

$$= \sum \mathcal{H}_p\mathcal{H}_q\, \Sigma_{\tilde{x}}(p,q), \tag{49}$$

for the cross terms, where $\mathcal{H}_p$ represents the impulse response of H_p. From Equation (48) to (49) Pareseval's equation was used [17].

Table II summarizes the worst-case and stochastic results for the quantization error on joint space, operational space, and joint and operational space derivative estimates.

IV. Experiment: Cartesian Position, Velocity, and Acceleration Error of the Phantom Premium Robot

Experiments with a Phantom Premium 1.5 haptic device/robot (SensAble Technologies, Inc.) were conducted to compare theoretical and experimental results. Two sets of experiments were performed to analyze the error from quantization in joint space. The first set tested the error distributions on operational space coordinates for various configurations of the robot. The second set analyzed the error distributions on operational space derivative signals. The joint and operational space coordinates of the robot are the standard coordinates for the Phantom Premium [18], and are shown in Fig. 4.

An input undergoes d back differences, and then n low-pass filters with a cut-off frequency of ω_0 (rad/s) and unity gain at zero frequency. Other filters could be used; this specific filter was chosen because of its simplicity and common implementation. The parameters of the filter are $d = 1$ (corresponding to

TABLE II
JOINT SPACE QUANTIZATION ERROR PROPAGATION SUMMARY

General	Independent PQN
$\lvert\tilde{\theta}\rvert \leq \frac{1}{2}\Delta$	$\mathbf{E}\tilde{\theta} = \mathbf{0}$ $\Sigma_{\tilde{\theta}}(i,i) = \frac{1}{12}\Delta_i^2$
$\lvert\tilde{\phi}_i\rvert \leq \lVert G_i\rVert_{\ell_1}\lvert\theta_i\rvert_{\max}$	$\mathbf{E}\tilde{\phi} = \mathbf{0}$ $\Sigma_{\tilde{\phi}}(i,i) = \lVert G_i\rVert_2^2\,\Sigma_{\tilde{\theta}}(i,i)$
$\lvert\tilde{x}\rvert \leq \frac{1}{2}\lvert J\rvert\Delta$	$\mathbf{E}\tilde{x} = \mathbf{0}$ $\Sigma_{\tilde{x}} = J\Sigma_{\tilde{\theta}}J^T$
$\lvert\tilde{y}_j\rvert \leq \sum_{i=1}^n \lvert J_{ji}\rvert\lvert\tilde{\phi}_i\rvert_{\max}$ $\lvert\tilde{y}_j\rvert \leq \lVert H_j\rVert_{\ell_1}\lvert\tilde{x}_j\rvert_{\max}$	$\mathbf{E}\tilde{y} = \mathbf{0}$ $\Sigma_{\tilde{y}} = J\Sigma_{\tilde{\phi}}J^T$ $\Sigma_{\tilde{y}}(j,j) = \lVert H_j\rVert_2^2\,\Sigma_{\tilde{x}}(j,j)$ $\Sigma_{\tilde{y}}(p,q) = \sum \mathcal{H}_p\mathcal{H}_q\Sigma_{\tilde{x}}(p,q)$

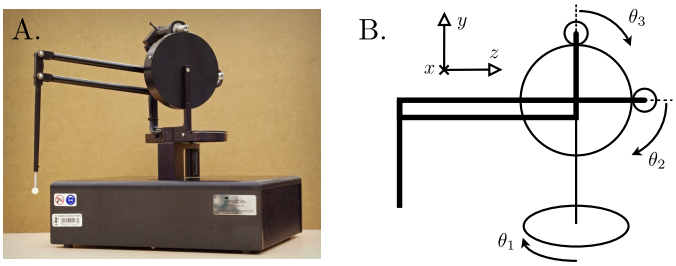

Fig. 4. A. The Phantom Premium 1.5 used in the experiment. B. A schematic of the Phantom Premium 1.5. The joint space coordinates are θ_1, θ_2, and θ_3, and the operational space coordinates are x, y, and z. The schematic displays the robot in the zero position. This figure is modified from [18].

velocity), a filter order of n = 1, a sample rate of 1000 Hz, and a cut-off frequency of 50 Hz. Because we use a linear model of the forward kinematics to obtain a local description of the error, an alternate filter in joint space (with the structure of G equivalent to H) would result in the same error on velocity.

A. Experimental Procedure

In both sets of experiments, the robot was controlled to oscillate about a given configuration with sinusoidal motion in which two types of signals were recorded: one with signals constructed from *artificially* quantized joint angles with a quantization interval of 1 milli-rad, and another without artificial quantization to create signals acting as truth. The actual quantization of the robot is 0.125 milli-rad for all joints, so the artificial quantization was 8 times the natural. The

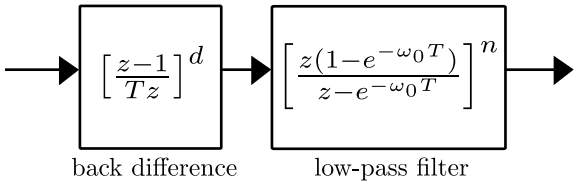

Fig. 5. The structure of the transfer functions, H_j, to form derivative signal estimates for Section IV. The input undergoes d back differences and n single order low-pass filters with cut-off frequency ω_0 (rad/s).

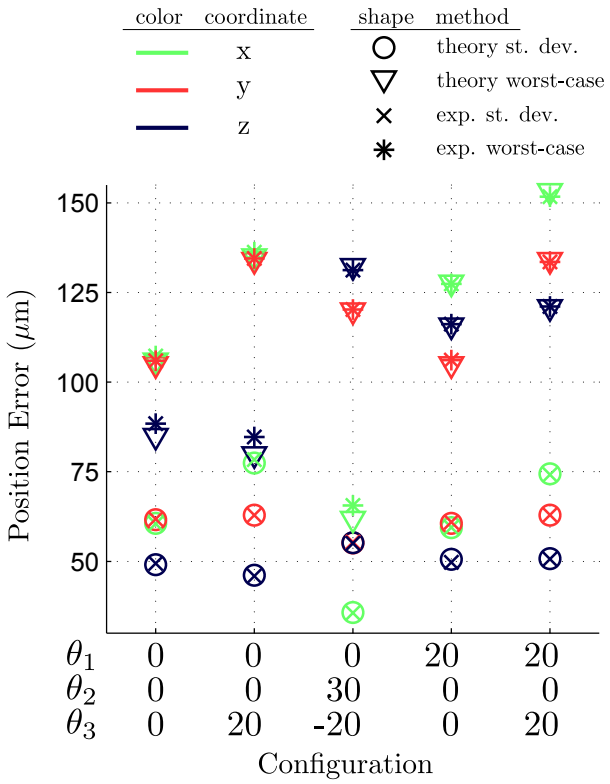

Fig. 6. The theoretical and experimental worst-case, and standard deviations of, the operational space coordinate error for various configurations (in degrees) of the Phantom Premium 1.5 used in the experiment.

amplitude of the motion, A, was 3° in each joint angle, and each joint had a different frequency, ω, within 0.1 Hz of 5 Hz to ensure independent error in joint space coordinates. All experiments were run with a control and data collection rate of 1 kHz, and a specific experiment was 15 seconds.

Because the robot was moving with amplitude sufficiently large compared to the quantization intervals, and the motion of the robot was sufficiently fast compared to the product of Δf, the PQN model is predicted to hold to a high degree of accuracy [1].

B. Error Distribution on Operational Space Coordinates

For the first set of experiments, theoretical and experimental results for the worst-case and standard deviation error for operational space coordinates in various configurations of the robot were found. The experimental error for an operational space coordinate (e.g., the x coordinate), was the difference between the signal constructed using the forward kinematics with artificial quantization and the one without. The results are displayed in Fig. 6 for various configurations of the robot. Matching the analytical results of Section III, the mean of the experimental error was close to zero for all experiments. The largest magnitude of the mean error for all experiments was less than 2μm.

C. Error Distribution on Operational Space Velocity and Acceleration

The second set of experiments examined the error on the velocity and acceleration estimates of an operational space

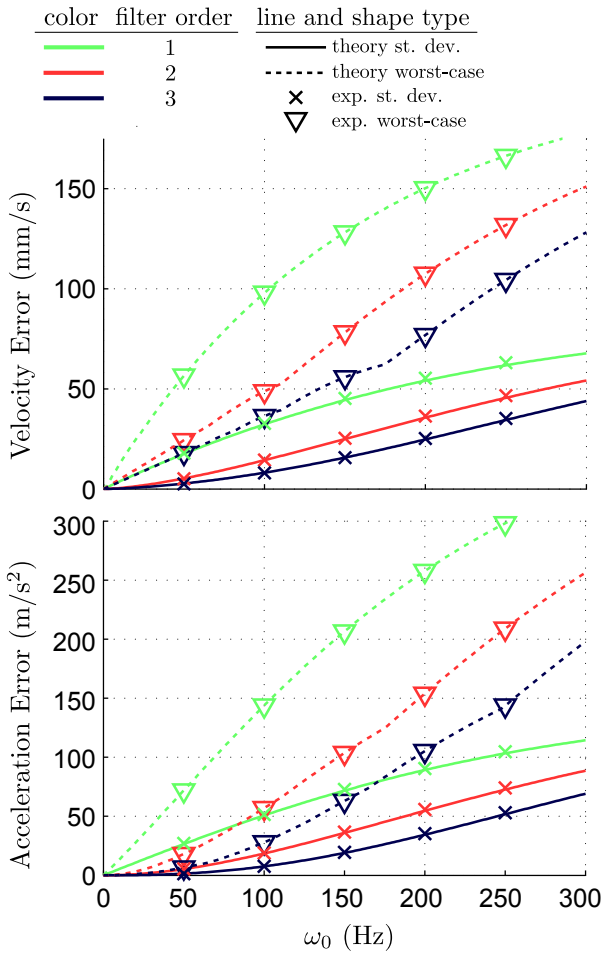

Fig. 7. The theoretical and experimental worst-case, and standard deviations of, the operational space coordinate derivative error about the zero position of the Phantom Premium 1.5 used in the experiment for various filter orders.

coordinate (the x coordinate) about the zero configuration for various filter orders. The error was formed by the difference between artificially quantized joint space coordinates and those without using the filter in operational space approach described in Fig. 2A. The structure of the transfer functions were that of Fig. 5, where the back-difference order, d, was 1 for velocity, and 2 for acceleration. The experimental mean, variance, and worst-case error was computed for various cut-off frequencies, ω_0, of the low-pass filter for three filter orders n = 1, 2, and 3, and compared to theoretical predictions. The results are displayed in Fig. 7. The mean of the experimental derivative error was small for all experiments; the largest magnitude of the mean of an error signal was less than 1% of its standard deviation for all experiments.

D. Comparison of Theory and Experiment

The minor discrepancies between the theory and experimental data present in Figures 6 and 7 come from two sources. The first source is that an affine model of the forward kinematics is used to analyze the error on operational space coordinates and estimates of their derivatives. Thus, the results for operational space are configuration dependent, and the region for which the results are valid is related to how well the forward kinematics are described by an affine model in a certain configuration. The second source of discrepancy between analytical predictions and experimental data, which applies only to the stochastic results, is the independent PQN model of quantization error.

V. Conclusion

We characterized quantization error in a robotic system. Given quantization specifications, robot kinematics, and discrete transfer functions mapping coordinates to their derivatives, we described the propagation of quantization error on joint space coordinates to operational space coordinates, joint space coordinate derivatives, and operational space coordinate derivatives. This work can be used by designers of robotics mechanisms and control engineers in order to predict the relationships between encoder quantization and the error on joint and operational space coordinates and their derivatives.

References

[1] B. Widrow and I. Kollár, *Quantization Noise: Roundoff Error in Digital Computation, Signal Processing, Control, and Communications*. Cambridge, UK: Cambridge University Press, 2008.

[2] W. R. Bennett, "Spectra of quantized signals," *Bell System Technical Journal*, vol. 27, no. 4, pp. 446–472, 1948.

[3] B. Widrow, "A study of rough amplitude quantization by means of nyquist sampling theory," *IRE Transactions on Circuit Theory*, vol. 3, no. 4, pp. 266–276, 1956.

[4] T. A. C. M. Claasen and A. Jongepier, "Model for the power spectral density of quantization noise," *IEEE Transactions on Acoustics, Speech and Signal Processing*, vol. 29, no. 4, pp. 914–917, 1981.

[5] I. Kollár, "Bias of mean value and mean square value measurements based on quantized data," *IEEE Transactions on Instrumentation and Measurement*, vol. 43, no. 5, pp. 733–739, 1994.

[6] A. Pacut, K. Hejn, and L. Kramarski, "Generalized model of the quantization error – analytical approach," in *International Workshop on ADC Modelling and Testing*, 1997, pp. 1–5.

[7] R. M. Gray, "Quantization noise spectra," *IEEE Transactions on Information Theory*, vol. 36, no. 6, pp. 1220–44, 1990.

[8] J. E. Bertram, "The effect of quantization in sampled-feedback systems," *Transactions of the American Institute of Electrical Engineers, Part II: Applications and Industry*, vol. 77, no. 4, pp. 177–182, 1958.

[9] A. V. Oppenheim, A. S. Willsky, and S. H. Nawab, *Signals & Systems*, 2nd ed. Upper Saddle River, NJ: Prentice-Hall, 1996.

[10] K. Zhou, J. C. Doyle, and K. Glover, *Robust and Optimal Control*. Upper Saddle River, NJ: Prentice-Hall, 1996.

[11] G. E. Dullerud and F. Paganini, *A Course in Robust Control Theory: A Convex Approach*. New York, NY: Springer, 2000.

[12] R. Kavanagh and J. M. D. Murphy, "The effects of quantization noise and sensor nonideality on digital differentiator-based rate measurement," *IEEE Transactions on Instrumentation and Measurement*, vol. 47, no. 6, pp. 1457–1463, 1998.

[13] R. Brown, S. Schneider, and M. Mulligan, "Analysis of algorithms for velocity estimation from discrete position versus time data," *IEEE Transactions on Industrial Electronics*, vol. 39, no. 1, pp. 11–19, 1992.

[14] S. M. Phillips and M. S. Branicky, "Velocity estimation using quantized measurements," Proceedings on *IEEE Conference on Decision and Control*, vol. 5, pp. 4847–4852, 2003.

[15] A. J. L. Harrison and D. P. Stoten, "Generalized finite difference methods for optimal estimation of derivatives in real-time control problems," Proceedings of the *Institution of Mechanical Engineers, Part I: Journal of Systems and Control Engineering*, vol. 209, no. 2, pp. 67–78, 1995.

[16] N. Colonnese and A. Okamura, "Stability and quantization-error analysis of haptic rendering of virtual stiffness and damping," *The International Journal of Robotics Research*, vol. 35, no. 9, pp. 1103–1120, 2016.

[17] J. C. Doyle, B. A. Francis, and A. R. Tannenbaum, *Feedback Control Theory*. Dover Publications, 2009.

[18] M. C. Cavusoglu, D. Feygin, and F. Tendick, "A critical study of the mechanical and electrical properties of the phantom haptic interface and improvements for high performance control," *Presence*, vol. 11, no. 5, pp. 555–568, 2002.